Morphology tailored SnO_2 thin films by spray gel process

Clemente Luyo[1], Luis Reyes[1], José Solís[1,2], Juan Rodríguez[1,2], Walter Estrada[1,2], Ismael Fábregas[3], Robert Candal[3]

[1] Universidad Nacional de Ingeniería. Facultad de Ciencias, Casilla 31-139, Lima, Perú
[2] Instituto Peruano de Energía Nuclear, Av. Canadá 1470, San Borja, Lima 41, Perú
[3] INQUIMAE-DQIAQF, Facultad de Ciencias Exactas y Naturales, Universidad de Buenos Aires, Ciudad Universitaria Pabellón 2, C1428EHA Buenos Aires, Argentina

Abstract

Nanostructured tin oxide films were prepared by depositing different sols using spray pyrolysis in a novel technique, the so-called spray-gel process. SnO_2 sols were obtained from tin alkoxide $Sn(t\text{-}OAm)_4$ or tin tetrachloride ($SnCl_4$ $5H_2O$) precursors and stabilized with ammonia or tetra-ethyl ammonium hydroxide (TEA-OH) as peptizers. Xerogels from the different sols were obtained by solvent evaporation under controlled humidity. The Relative Gelling Volumes (RGV) strongly depend on the type of precursor. Xerogels obtained from inorganic salts gelled faster, while, as determined by TGA, occluding a significant amount of volatile compounds. Infrared spectroscopic analysis was performed on raw and annealed xerogels (500 ^oC, 1h). Annealing removes ammonia or alkyl ammonium hydroxide, increasing the number of Sn-O-Sn bonds. SnO_2 films were prepared by spraying the sols for 60 min onto glass and alumina substrates at 130°C for 60 min. The films obtained from both precursors were amorphous or had a very small grain size, and crystallized after annealing at 400°C and 500^{o}C in air for 2 h. XRD analysis showed the presence of the cassiterite structure and line broadening indicated polycrystalline material with a grain size in the nanometer range. SEM demonstrated a strong dependence of the film morphology on the RGV of the sols. Films obtained from $Sn(t\text{-}OAm)_4$ present a highly textured morphology based on fiber-shape bridges, whereas the films obtained from $SnCl_4$ $5H_2O$ have a smoother surface formed by "O-ring" shaped domains. The performance of the films in gas sensor devices was tested. The conductance response for ethanol was of the same order of magnitude for the three kinds of films. The response of the highly textured films was more stable with shorter response times.

1. Introduction

Tin dioxide-based films have found various applications, the most important being for gas sensors [1], catalysts [2], transparent conductive electrodes [3], etc. The microstructure of the films plays an important role in the physico-chemical properties of the material. In the particular case of gas sensors, a chemical species adsorbed on the semiconductor surface yields an electrical signal that is transduced through the microstructure of the sintered film, producing a conductance change. Grain contacts, as well as the grain size in the oxide semiconductor microstructure, constitute key features for the transducer function [1a, 1b, 4]. The surface-to-bulk ratio for a nanocrystalline material is much larger than for a material with coarse grains [5], which may result in an improvement of the system performance [6]. Besides, it was recently reported that the sensing activity of films depends on several factors such as the crystallite shape, microscopic structure, crystallographic orientation of crystallite planes and inter-crystallite necks (see [7] and references therein).

A number of methods have been developed to synthesize nanocrystalline SnO_2 films; of these, the sol-gel [8] and spray pyrolysis [9] techniques have been extensively employed due to their low cost and simplicity. Even though nanocrystalline films have been obtained by spray pyrolysis or sol gel techniques, their surface morphologies were not very rough. A new method, known as the spray-gel process, that results when both the spray pyrolysis and the sol-gel techniques are carefully combined, has been used to modify the film's morphology by controlling the precursors and deposition conditions [10]. The process consists basically of producing an aerosol from a sol, which is subsequently sprayed onto a hot substrate, where the film grows.

The synthesis of films by techniques that use diluted solutions or a suspension containing the precursors, involves the elimination of a considerable amount of solvent. Such is the

case with sol-gel, spray-pyrolysis or spray-gel methods. This situation has unwanted environmental consequences if the solvent is an organic compound (typically an alcohol) or, in the case of spray-pyrolysis, if important amounts of hydrochloric or nitric acids are released to the atmosphere. The use of aqueous-based sols, such as those utilized in the present work, mitigates the consequences of solvent evaporation because water is environmentally benign and, perhaps even more relevant, is cheaper than alcohol.

In this work, we have used this route to tailor the morphology of nanocrystalline SnO_2 films using the spray-gel technique. We describe the effect of the composition of the sols on the sol-gel transition and the characteristics of the xerogels and films. The ethanol sensing ability of sensor devices prepared with the different sols is also presented.

2. Experimental

2.1 Synthesis of SnO_2 sols

Three different SnO_2 sols were prepared by the precipitation–peptization method. $SnCl_4.5H_2O$ was used as Sn(IV) precursor for the sols named I and T, while tin tetra tert-amyloxide ($Sn(t\text{-}OAm)_4$) was used as precursor for sol A. Ammonia was used as basic catalyst for the hydrolysis of the SnO_2 precursors. Tetraethyl ammonium hydroxide (TEA-OH Aldrich) was used as peptizer for sol T.

To prepare sol I, 7 g of $SnCl_4.5H_2O$ (Carlo Erba, pa), sufficient to yield a 2% SnO_2 final suspension was dissolved in 100 mL of water (MilliQ) (solution 1). 5 mL concentrated ammonia (Merck, pa) were added to 100 mL of water pre-heated to 60 ºC (solution 2). Solution 1 was added rapidly to solution 2 under strong stirring. A white precipitate was formed in less than 5 min. The suspension was stirred for 30 minutes at 60 ºC, after which it was allowed to cool to room temperature and centrifuged to separate the precipitate from the supernatant liquid. The solid was dispersed in pure water using an ultrasonic bath and re-centrifuged. This washing procedure was repeated twice to reduce the amount of ammonium chloride remaining in the solid. After the last wash, the SnO_2 was dispersed in 100 mL of water and the pH adjusted to 9 with a 5 M NH_3 solution. Finally, the suspension was placed in an ultrasonic bath for 60 minutes during which a stable SnO_2 sol was obtained.

The synthesis of sols A and T were similar, but $Sn(t\text{-}OAm)_4$ was used instead of $SnCl_4.5H_2O$ for sol A, and 5% TEA-OH (Aldrich) solution was used to prepare the final dispersion and to adjust the pH to 9.0 (sol T, only). $Sn(t\text{-}OAm)_4$ was synthesized in the laboratory from anhydrous $SnCl_4$, by exchanging Cl for tert-amyloxide under an inert atmosphere. In this case, ethylenediamine was used to neutralize HCl [11]. Sol A was prepared by dispersing a heptane 0.4 M solution of $Sn(t\text{-}OAm)_4$ into water alkalinized to pH 8 with ammonia. The white precipitate was separated by centrifugation and washed twice with pure water. A stable sol was obtained by adjusting the pH to 9.0.

2.2 SnO_2 xerogels

SnO_2 xerogels were prepared by drying a suitable amount of the above-mentioned sols at 33% relative humidity (over $MgCl_2.6H_2O$ saturated solution, 25 ºC). The volumes of the sols at the gelling point were measured. The Relative Gelling Volume (RGV), defined as the percentage of the gel volume to initial sol volume, was then calculated. Approximately 2/3 of the xerogels were fired at 300 or 500 ºC for 1 hr (rate 4ºC min^{-1}) to produce membranes. The remaining 1/3 was used without further thermal treatment. The fired and raw xerogels were characterized by X-ray diffraction (XRD), Fourier transform infrared spectroscopy (FTIR), thermogravimetric (TGA), difference thermal analysis (DTA) and surface area by BET method. The xerogels and membranes were characterized by infrared spectroscopy and thermogravimetry using a Fourier transform infrared spectrophotometer Nicolet 320 and a TGA-51 Shimadzu, respectively.

DRX of the ground xerogels or membranes were performed in a Siemens D-5000 difractometer operating with CuK_α radiation, and the FTIR analysis was performed using a Fourier transform infrared spectrophotometer Nicolet 320. Samples of xerogels and KBr (Merck, pa) were ground in an agate mortar in order to prepare a 5 % mix of both components. The mixture was compressed (~ 2 atm) under vacuum in a specially designed sample holder in order to prepare KBr pellets containing the sample.

TGA and DTA analysis were performed in a Shimadzu TGA-51 and a DTA 50, respectively. The heating ramp was held in 2 ºC/min in both cases; the analyses were run under air or nitrogen atmosphere as indicated in the text. Specific surface areas were estimated by measuring N_2 adsorption isotherms on a Gemini 2360 V2 apparatus.

The concentration of chloride ions was measured potentiometricaly with a specific

ion electrode (Orion, 94-17A) using the standard incorporation method.

2.3 SnO_2 thin films

An outline of the spray system used in this work has been described elsewhere [12]. The spray-gel technique was used to obtain tin oxide films on either alumina substrates or glass slides. The sols prepared as described above were sprayed onto the substrates heated at 130 °C for 1 h. The gas carrier flux and air pressure were kept at 40 L/min and $1.5x10^5$ Pa, respectively. Further stabilization of the films was accomplished after annealing at 400 ºC for 2 h.

The crystal structure and crystallite size of the nanocrystalline SnO_2 films were characterized by x-ray diffraction, using a Phillips X Pert diffractometer operating with CuK_α radiation. The microstructures of the films were analyzed by using a scanning electron microscope (SEM) Hitachi S500.

For gas sensing studies, the SnO_2 films were deposited onto alumina substrates using preprinted gold electrodes, 0.3 mm apart, and a Pt-heating resistor on the reverse side. The samples to be tested were placed in a stainless steel chamber (4.4 L) and exposed to different ethanol vapor concentrations. The obtained films that bridged the gold electrodes were connected in series with a known resistor. In this scheme, the conductance was obtained by measuring the electric current through the film at a constant voltage of a 5.0 V. The gas-sensing properties of the films were studied at 400 °C.

3. Results

3.1 SnO_2 sols

Upon mixing the precursor solutions at 60 ºC white flocks of SnO_2 appeared immediately; the precipitate settled rapidly if the stirring was stopped. In the case of sols I and T, after precipitation the pH´s of the suspensions were close to 2.5 and $[Cl^-]$ = 0.53 M. The pH of the suspension obtained by dispersing the SnO_2 precipitate, previously rinsed with pure water, in 5% NH_3 was ~ 8 and the $[Cl^-]$ = 0.033 M. Under these conditions, an incipient peptization of the precipitate was observed, although a stable sol could not be produced in spite of the application of ultrasound for several hours. Complete peptization of the SnO_2 precipitate was obtained once the pH was adjusted to 9.0 with either 5M NH_3 or 5M TEA-OH. At this pH and ionic strength the sols were stable for weeks; the small amount of SnO_2 that settled with time could be re-suspended easily by application of ultrasound. During the experiments, it was demonstrated that pH has the major influence on sol stability. If, after the first rinsing, the pH increased to 5, most of the SnO_2 remained in suspension in spite of the high chloride concentration ($[Cl^-]$ = 0.053M).

In the case of sol A, after precipitation the pH was close to neutral because no acid is produced during the hydrolysis of $Sn(tAmO)_4$. A small amount of ammonia was needed to adjust the pH to 9.0.

Table 1 shows the RGV for the three prepared sols. Sol I displays the highest RGV, followed by sol T and sol A. It should be noticed that the higher the RGV the higher the amount of solvent that remains included in the gel and xerogel.

Table 1. The Relative Gelling Volumes (RGV) for different sols.

Sol	I	T	A
Precursor	$SnCl_4.5H_2O$	$SnCl_4.5H_2O$	$Sn(t\text{-}Oam)_4$
Peptizer	NH_3	TEA-OH	NH_3
RGV (%)	81	56	25

3.2 SnO_2 membranes

Figure 1a shows TGA traces for the three membranes; these analyses were performed in air. In agreement with RGV data, Xerogel I contains the highest amount of volatile compounds included in the gel network (64%), followed by xerogel T (37.5%) and A (14%). Figure 1b shows DTA traces for the same xerogels performed under normal laboratory atmosphere. In the case of xerogel T, the experiment was also performed under a nitrogen atmosphere.

Xerogel A displays the simplest decomposition pattern, with only one major loss of mass at ~50 ºC. The DTA trace for xerogel A shows a small endothermic feature at ~ 50 ºC which indicates that the loss of mass observed at the same temperature in the TGA curve corresponds to an endothermic process, most likely water or alcohol evaporation. Xerogels I and T display a more complicated pattern of decomposition; the volatile compounds were eliminated in several steps at different temperatures. In the case of xerogel T, there is a marked loss of mass in the range 40-120 ºC, that can be associated with an endothermic process indicated by the feature centered at 85 ºC in the DTA analysis (Figure 1b). As in the previous case, the loss of mass can be associated with water evaporation, corresponding to ~ 13% of the initial mass. In the range 180-255 ºC there is an important loss of mass (15.6%) that corresponds to an endothermic process followed by an

exothermic process characterized by a sharp peak centered at 247 ºC (see Figure 1b). When the DTA analysis was performed under nitrogen, only the endothermic process was clearly observed, followed by a wide and poorly defined exothermic feature. These results indicate that the sharp peak observed under air corresponds to an oxidation process. This oxidation is likely to be associated with the combustion of the TEA alkyl chains. In the range 255-375 ºC there is another loss of mass, which corresponds to ~ 4.5% of the initial mass, associated with a sharp exothermic peak centered at 345 ºC. This process is related with oxidation of the carbon that remains in the sample, probably inside the open pores of the sample. The final loss of mass in the range 375-700 ºC may be associated with a wide exothermic peak centered at 420 ºC. This process could be connected with loss of structural water.

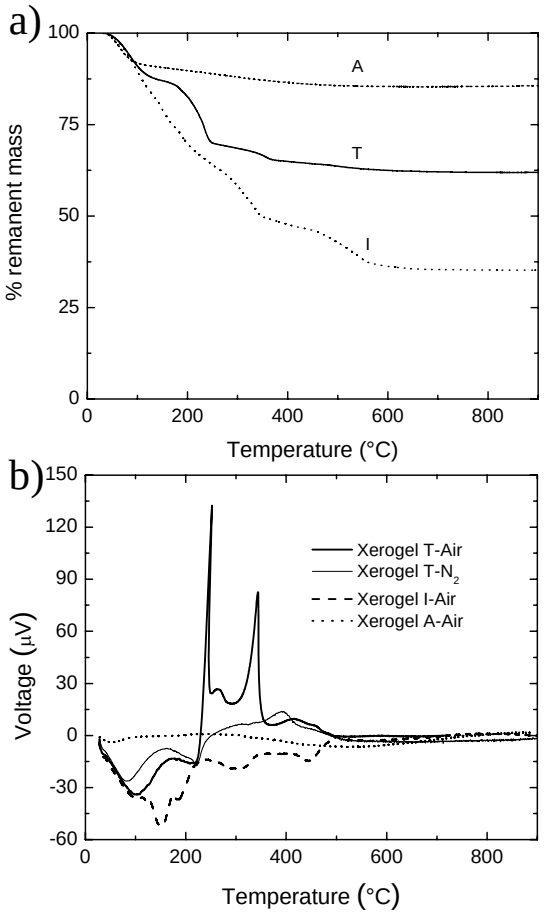

Figure 1. (a)TGA profiles for SnO_2 xerogels from inorganic (I and T) and metal alkoxide (A) precursors. (b) (a) DTA profiles for SnO_2 xerolgels from inorganic (I and T) and metal alkoxide (A) precursors. Experiments were performed in air or in N_2 atmosphere as indicated.

Figure 1a shows that, in the case of Xerogel I, there is a continuous loss of mass, with changes in the slope of the curve, as the temperature increases from 25 to 350 ºC. The changes in the slope indicate that several processes contribute to the loss of mass. In greement, Figure 1b shows that the DTA analysis displays various endothermic peaks that can be correlated with the mass loss observed by TGA. In the range 25-100 ºC the loss of mass is similar to that observed for sol T, and corresponds to an endothermic process (see Figure 1b), probably the elimination of physisorbed water. In the range 100-450ºC there are several endothermic processes that include elimination of water and ammonium chloride. Figure 1a also shows a loss of mass centered at 500ºC that corresponds to an exothermic feature in the DTA analysis. This process may be related with elimination of water of constitution and further cross linking of the structure.

Figure 2a, b and c, shows, respectively, the IR spectra of the xerogels obtained from sols I, T, and A fired at different temperatures. The IR features at 3050 and 1400 cm^{-1} shown in Figure 2a indicate the presence of ammonium (probably ammonium chloride) in the as-obtained xerogel. As the temperature increases, the intensity of the features decrease, being almost negligible at 300 ^oC and disappearing completely at 500 ^oC. These results indicate that ammonium is mostly eliminated at temperatures in the range 300-400 ^oC. Features at 1100-1400 cm^{-1} (C-H, N-C stretching) and 2900 cm^{-1} (C-H stretching) present in Figure 2b, indicate the presence of tetraethylammonium in the as-obtained xerogel T. The intensity of the peaks in the sample fired at 300 ^oC is very low, indicating that most of the TEA is eliminated at this temperature. This result agrees with the loss of mass observed in the TGA, as was discussed above. The features in Figure 2c indicate that raw xerogel A contains ammonium and water, although the presence of alkoxide groups cannot be excluded due to the broad bands in the range 1250-900 cm^{-1}. The intensity of the peaks is much smaller than in the previous cases, due to the lower amount of volatile compounds occluded in this xerogel (see Figure 1). It should be noted that, in the three raw xerogels (see Figure 2 a, b and c), a feature at 550 cm^{-1} may indicate the presence of Sn-OH bounds. As the firing temperature increases, the intensity of this feature decreases and another feature at 650 cm^{-1}, corresponding to Sn-O-Sn bounds, systematically increases. These changes are associated with the loss of water of constitution, and are in accordance with the loss of mass observed at 400-500 ^oC by TGA.

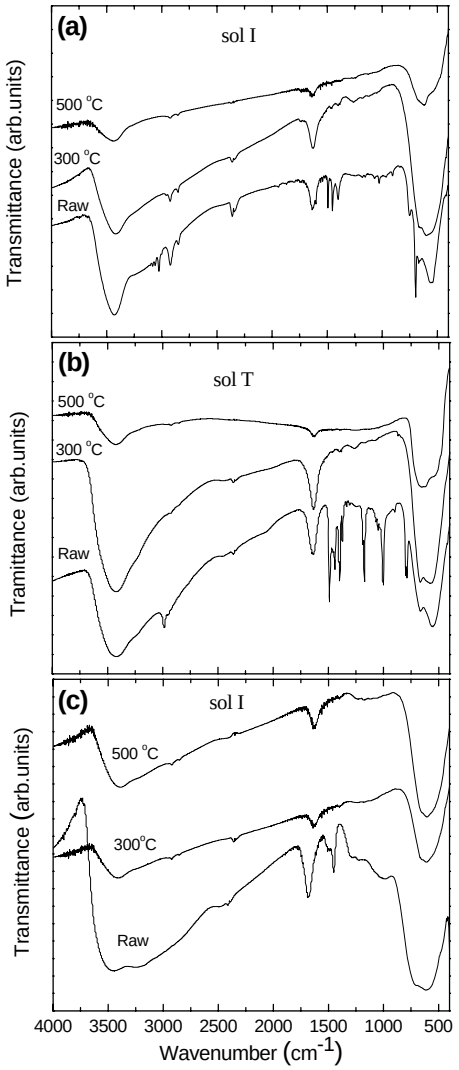

Figure 2. FTIR spectra of SnO_2 xerogels from inorganic I (part a), T (part b) and metal alkoxide (A) (part c) precursors. As deposited, annealed at 300 °C for 1 h and annealed at 500 °C for 1 h.

Figure 3 shows XRD patterns of the xerogel fired at different temperatures. In all cases the typical pattern of cassiterite was obtained. However, the crystallinity of the unfired xerogel was considerably lower than in the fired samples. Table 2 shows the grain size estimated from the Scherrer equation [15]. In all cases the crystallites growth notoriously as the temperature change from 300 to 500 °C.

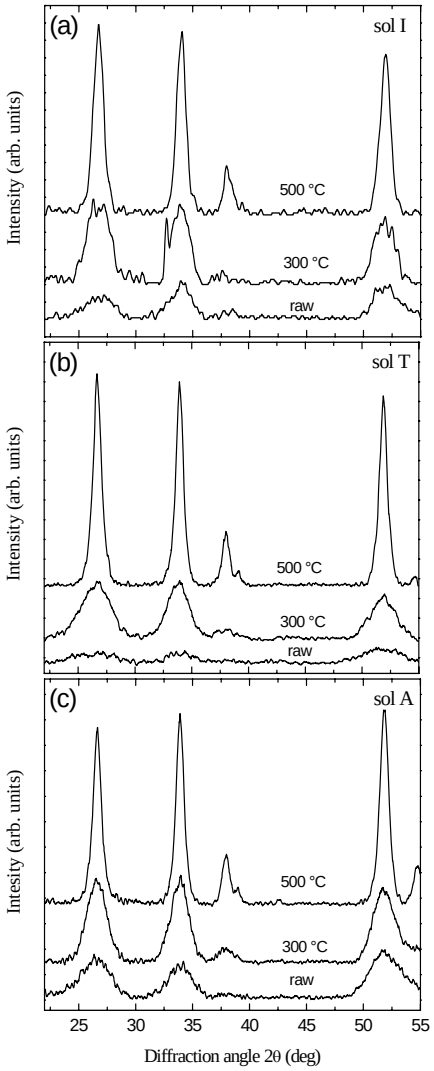

Figure 3. X-ray diffraction patterns of SnO_2 xerogels from inorganic I (part a), T (part b) and metal alkoxide (A) (part c) precursors. As deposited, annealed at 300 °C for 1 h and annealed at 500 °C for 1 h.

Table 2. Grain size estimated from the Scherrer equation for raw and annealed xerogels from different sols.

	Xerogel I	**Xerogel T**	**Xerogel A**
raw	5.8	4.6	5.4
300 °C	5.9	6.9	7.9
500 °C	14.9	18.9	19.5

Table 3 shows that the specific surface areas of the xerogels decrease as the firing temperature increases; xerogel T displays the higher surface area while xerogel A displays the lower one. These results agree with the

changes in the grain size previously described.

Table 3. The specific surface areas of the annealed xerogels from different sols.

Xerogel	I	T	A
300 °C	179	221	134
500 °C	42	43	34

3.3 SnO_2 Thin films

X-ray diffraction patterns for SnO_2 films obtained from sol T and sol I in an as-deposited state and after annealing at 400 ºC and 500 ºC for 2 h, respectively are shown in Fig. 4. The diffraction patterns showed that the as-deposited SnO_2 films were amorphous or with a very small grain size. The X-ray diffraction patterns for films after annealing at a temperature of 400 °C revealed the presence of the cassiterite structure. Line broadening obtained after substration of the glass substrate background of the film, indicates that the films are polycrystalline with grain size in the nanometer range ~ 10 nm, according to Scherrer´s equation. The films obtained from sol A show similar behavior.

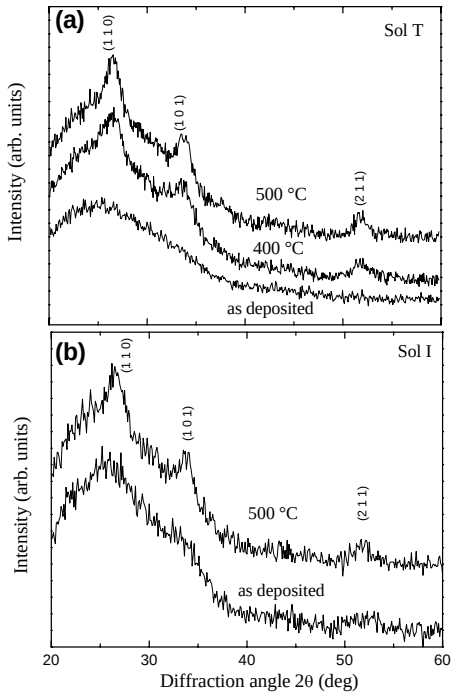

Figure 4. X-ray diffraction patterns for SnO_2 films made from sol T (part a) and I (part b) as deposited, and after annealing at 400 and 500 ºC for 2 h.

The SEM micrographs of the as-deposited and post-annealed (500 °C for 2 h) SnO_2 films obtained from sols I, T and A, are shown in Figs. 5, 6 and 7, respectively. Figure 5a displays the morphology of the as-deposited and annealed SnO_2 films obtained from sol I. The as-deposited SnO_2 film is composed of well-defined "O-ring shaped" domains of ~15 μm diameter with a rough surface. After annealing, the surface of the films becomes smoother, see Fig. 5b.

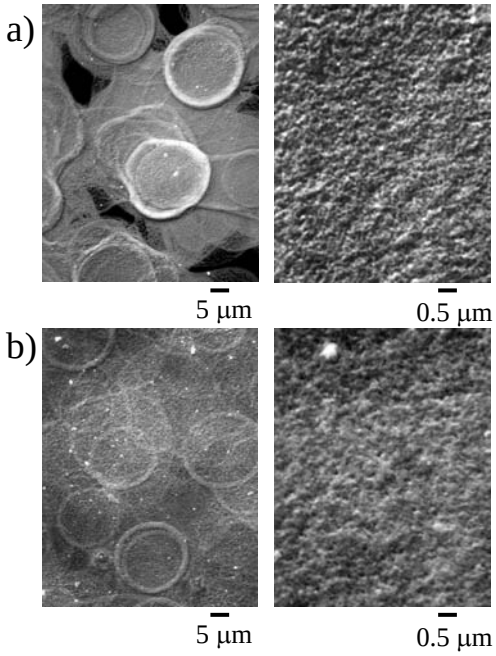

Figure 5. High and low magnification SEM micrographs for SnO_2 films obtained from sol I, as deposited (a) and after annealing at 500 ºC (b).

The surface of the as-deposited SnO_2 film from sol T is also rough (Fig. 6a). However, in this case, the structured circular domains are not as well-defined as in the previous case. After annealing (Fig. 6b), the surface of the films becomes smoother and domain borders almost disappear (Fig. 6b). A typical SEM micrograph of a SnO_2 film obtained from sol A is presented in Figure 7. The as-deposited film shows a morphology based on very well defined "O-ring shaped" domains, In this case however, in contrast to the sol I films, the domains seemingly intersect each other and constitute a complicated pattern of interconnected fibers distributed uniformly throughout the film surface (Fig. 7 a). After annealing, the number of rings increases, giving highly textured films (Fig. 7 b). The studied films exhibit different degrees of texture, as observed by SEM. The surface of the annealed films obtained from an inorganic precursor is less textured than the surface of films obtained from a metal alkoxide precursor. Figure 8 shows the cross section of the films obtained at 130 °C for 60 min. The film thicknesses vary, being, in the case of sol A, thicker and more textured.

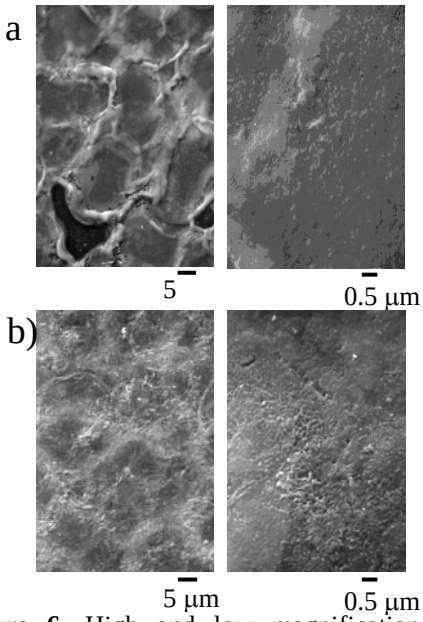

Figure 6. High and low magnification SEM micrographs for SnO_2 films obtained from sol T as deposited (a) and after annealing at 500 ºC (b).

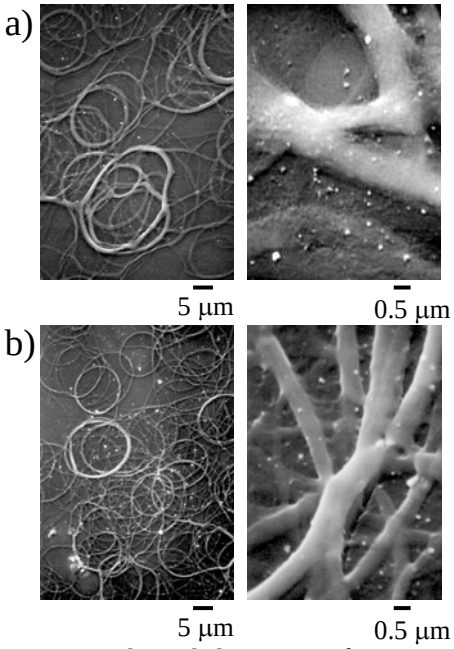

Figure 7. High and low magnification SEM micrographs for SnO_2 films obtained from sol A, as deposited (a) and after annealing at 500 ºC (b).

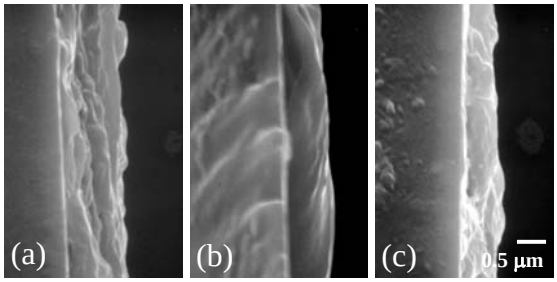

Figure 8. Cross section of the annealed SnO_2 films, obtained from (a) sol A, (b) sol I, and (c) sol T.

The films annealed at 500°C were used for gas-sensing experiments. Figure 9 shows the film conductance in response to different concentrations of ethanol in air. In general, all films respond to the presence of ethanol, with signals of the same order of magnitude. However, the response of the highly textured films obtained from metal alkoxide (sol A) was more stable and had a shorter response time. The other films (sol I and T) were unstable and had lower response times than the most textured ones.

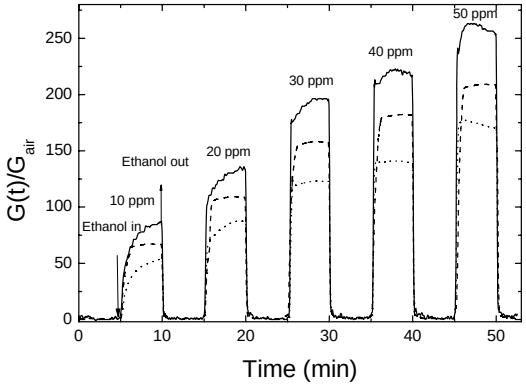

Figure 9. Conductance response, $G(t)/G_{air}$ as a function of time of SnO_2 films from sol T (solid line), sol I (dotted line) and sol A (dashed line), after annealing at 500 ºC, subjected to different ethanol concentrations in air at 400 °C.

4. Discussion

The reactions taking place during hydrolysis depend on the precursors; for sols I and T:

$$SnCl_4.5H_2O + 4NH_3 \rightarrow SnO_2 + 4NH_4Cl \quad (1)$$

And for sol A:

$$Sn(t\text{-}AmO)_4 + 4H_2O \rightarrow SnO_2 + 4t\text{-}AmOH \quad (2)$$

For sols I and T NH_4Cl is the main by-product, while for sol A *t*-AmOH is the main by-product.

As shown above, the stability of the sols strongly depends on pH and ionic strength. The effect of pH is related to the pH zpc (zero point charge) of the SnO_2, which is close to 4.5. At pH 9, the surface of the SnO_2 particles is negatively charged resulting in electrostatic repulsion. However, the presence of peptizers and the remaining by-products also affects some properties of the sols; for example their RGV values are notably different (see Table 1).

The high RGV value for sol I may be a result of sol destabilization produced by the presence of approximately 0.033 M ammonium chloride in solution. As the solvent is evaporated to produce xerogels, the

concentration of NH_4Cl increases. Increments in the electrolyte concentration reduce the double layer thickness, diminishing the inter-particle repulsion. Both processes, solvent evaporation and diminution of inter-particle repulsion, lead to gelation of the sol [13]. When gelation occurs in sol I, an important amount of water and ammonium chloride is occluded inside the gel. These volatile compounds are eliminated during the thermal treatment of the xerogel in several steps involving endothermic processes, as shown in Figure 1. FTIR analysis indicates that NH_4Cl is mostly eliminated in the range 300-400 ºC and water is eliminated at 450-500 ºC through oxolation reactions that increase the number of Sn-O-Sn bonds, as manifested by the increment of the intensity of the corresponding band in the FTIR spectra (see Figure 2). The de-hydroxylation of the xerogel leads to an increment in grain size and to an important reduction of surface area, as shown in Tables 2 and 3.

It was reported ([14]), that tetraethylalkyl ammonium cations could stabilize polyanions in solution and the effect was used to synthesize stable sols of TiO_2. In the case of sol T, the hydrophobic alkyl chains of the TEA^+ cation adsorbed on the sol particles and avoid their aggregation by steric interaction; gelation takes places when a fraction of solvent larger than in the case of sol I has been removed. The presence of TEA^+ also has important consequences on the microstructure of the xerogel. The surface area of this xerogel at 300 ºC is notably larger than that of xerogels I and A (see Table 3). This phenomenon could be a consequence of the presence of organic matter in between the particles. The organic matter diminishes the contact between particles, hindering aggregation and further crystal growth. When all the organic matter is eliminated at ca 400ºC (as indicated by TGA and FTIR analysis; see Figure 1a and 2b), the contact between particles increases, leading to oxolation processes that produce dehydration followed by crystallization of the xerogel (see Figures 1a, 2b and Table 2).

In the case of sol A, prepared from alkoxides and consequently free of salts, the thick electric double layer and high interparticle repulsion leads to the very low RGV. The possible presence of alkyl chains on the surface of the particles may also increase the repulsion between particles and sol stability. Due to the high stability of the sol, it is necessary to remove a considerable amount of solvent before the particle-particle interaction necessary for gel formation is reached. Consequently, the xerogel produced from this sol has the lowest amount of volatile compounds, the particles are packed very closely and the surface area is the lowest at all the temperatures studied.

The results discussed above have important consequences on the final morphology of the films. The amount of solvent that needs to be eliminated to obtain a gel depends on the type of sol, in the case of sols with high RGV, the amount of solvent that has to be evaporated before gelification is low and the sol-gel transition occurs rapidly once the sol reaches the hot surface of the substrate. Under similar conditions of film formation, sol I will produce gel-films faster than T and A.

The morphology of the films can be explained on the basis of the so-called “coffee drop deposition” (see Y. O. Popov [16] and references therein) and the gelation behavior of the sols. As the droplets of sprayed sol touch the hot surface of the substrate, the solvent (water) starts to evaporate. The droplet are bounded by their contact line in the plane of the substrate. The contact line remains pinned during most of the drying process [17]. Evaporation is faster at the edges and a solvent flow from the interior to the border is established; the particles concentrate at the border and a gelled foot forms near the drop edge [18]. In the case of sol I, due to the high RGV, further water evaporation leads to the gelation of all the drops. As a consequence the drops acquire the shape of a flat cylinder with engrossed borders. In the case of sol A, due to the low RGV, the gel is produced only at the borders where the particles concentrate due to the solvent flow. This process leads to the production of O-Ring domains with well defined walls. During firing at 500 ^oC, the O-rings interconnect with each other, producing the fibrous morphology displayed in Figure 7b. From Figure 6; it seems that sol T behaves as an intermediate case between sols A and I. This behavior is in agreement with its intermediate RGV value (Table 1). The borders look poorly defined, probably due to the accumulation of viscous TEA-OH at the edges. As demonstrated by TGA and DTA, TEA-OH decomposes at temperatures higher than 300 ^oC.

The gas sensing properties of SnO_2-based sensors for reducing gases are influenced by intrinsic and extrinsic factors. The intrinsic kind is related to the chemical composition and the second kind to the grain size and microstructure. The effect of the extrinsic factors on the sensing performance is related to the accessibility of inner oxide grains to the target gas [4, 19]. It was postulated that small thickness and large grain sizes improve the performance and sensitivity of the devices [1a]. In our case, the grain sizes of the films

are quite similar; this explains why the responses are similar. However, in agreement with the previous reports, the highest sensitivity was displayed by the device obtained from sol T, which has a lower thickness (see Figure 8) and larger grain size (see Table 2 and Figure 4). On the other hand, the sensor made from sol I showed the worst performance and the higher thickness and lower grain size. In the case of sol A, the film displayed an open macrostructure (see Figure 7) that may facilitate the diffusion of the ethanol molecules into the film, leading to a more stable response.

5. Conclusions

Nanocrystalline SnO_2 films were obtained by the spray-gel technique. Combining the spray pyrolysis and the sol-gel techniques (spray-gel) allows films with different macrostructures to be prepared. The morphology of the films strongly depends on the properties of the sol. The relation between sol RGV and film morphology can be described by the "coffee drop model". The performance of the films in sensor devices followed the expected trends with grain size and thickness. The open microstructure produced a more stable response.

6. Acknowledgements

This work was financially supported by the International Program for Physical Science of Uppsala University, Sweden (IPPS), the Research Institute of Universidad Nacional de Ingeniería, the CONCYTEC (Peruvian Research Council), University of Buenos Aires (UBACyT; TX 117), ANPCyT (Agencia nacional de Promoción de Ciencia y Tecnología) PICT 10621 and CYTED network VIII-G.

7. References

1. N. Yamazoe, Sensors and Actuators B 108 (2005) 2-14; b) N. Yamazoe, Sensors and Actuators B **7**, 7 (1991); c) W. Göpel, K.D. Schierbaum, "Electronic Conductance and capacitance Sensors", chapter 9, pp 430, in "Sensors: a comprehensive Survey, W. Göpel, J. Hess, J.N. Zenel, Ed., Vol 2, VCH (1991); d) J. Watson, Sensors and Actuators **5**, 29 (1984).

2. a) K. Tabata, T. Kawabe, Y. Yamaguchi, E. Suzuki, T. Yashima; J. Catalysis, 231 (2005), 438-437; b) M. J. Fuller and M. E. Warwick, J. Catalysis **29**, 441 (1973)

3. a) J. P. Chatelon, C. Terrier, J. A. Roger, Semicond. Sci. Technol, 14 (1999) 642-647; b) J. C. Manifacier, Thin Solid Films, **90**, 297 (1982).

4. D. D. Vuong, G. Sakai, K. Shimanoe, N. Yamazoe; Sensor and Actuators B 105 (2005), 437-442.

5. a) H. Gleiter, Mater. Sci. Forum **189-190**, 67 (1995); b) R.W. Siegel, Mater. Sci. Forum **235-238**, 851 (1997)

6. a) M.J. Madou and S.R. Morrison, *Chemical Sensing with Solid State Devices* (Academic Press, San Diego, 1989); b) N. L. Wu, S. Y. Wang, I. A. Rusakova; Science, 285 (1999), 1375-1377.

7. G. Korotcenkov, Sensors and Actuators B 107 (2005) 209–232.

8. a) J.P. Chatelon, C. Terrier, E. Bernstein, R. Berjoan, J.A. Roger; Thin Solid Films, 247, 162-168 (1994). b) S.S. Park, J.D. Mackenzie; Thin Solid Films, 258, 268-273 (1995). c) J.P. Chatelon, C. Terrier, J.A. Roger; Semicond. Sci. Technol., 14, 642-647 (1999).

9. D.R. Acosta, E. P. Zironi, E. Montoya, W. Estrada, *Thin Solid Films*, **288** (1996) 1-7.

10. (a)A. Medina, J.L. Solis, J. Rodriguez, and W. Estrada, Sol. Energy Mater. Sol. Cells **80**, 473 (2003), (b) M.A. Damian, Y. Rodriguez, J.L. Solis, and W. Estrada, Thin Solid Films **444**, 104 (2003).

11. I. Thomas, Methods for producing stannic tertiary alkoxide, U.S Patent 3 946 056.

12. J. Arakaki, R. Reyes, M. Horn, and W. Estrada, Sol. Energy Mater. Sol. Cells. **37**, 33 (1995).

13. C.J. Brinker, G.W. Scherer; "Sol-Gel Science", Academic Press INC, 1990.

14. Introduction to sol-gel Processing, Alain C. Pierre, Kluwer Academic Press, 1998. Chapter 3 "Colloidal Particles and Sols", pag153.

15. B.D. Cullity, Elements of X-ray diffraction, Addison-Wesley, Reading, MA, 1959.

16. Y. O. Popov, Phys. Rev. E, 71 (2005) 036313.

17. R. D. Deegan, O. Bakajin, T. F. Dupont, G. Huber, S. R. Nogel, T. A. Witten; Phys. Rev. E 62 (2000) 756.

18. F. Parisse, C. Allain, Langmuir, 13 (1997), 3598-3602.

19. D.D. Vuong, G. Sakai, K. Shimanoe, N. Yamazoe; Sensors and Actuators B 103 (2004) 386-391.